Coolability Evaluation of a Molten Salt Pool in MSR Containment Vessel under Decay Heat

*Jaemin Han[a], Ye Hwan Chun[a], JinHo Song[a], and Sung Joong Kim[*a,b]*
[a]Department of Nuclear Engineering, Hanyang University, 222 Wangsimni-ro, Seongdong-gu, Seoul 04763, Republic of Korea
[b]Institute of Nano Science and Technology, Hanyang University, 222 Wangsimni-ro, Seongdong-gu, Seoul 04763, Republic of Korea
**Corresponding author: sungjkim@hanyang.ac.kr*

***Keywords:** molten salt reactor, molten salt pool, natural convection, solidification, computational fluid dynamics

1. Introduction

The molten salt reactors (MSRs) have attracted attention as Generation IV reactor concepts. Compared with pressurized water reactors (PWRs), MSRs can operate at high temperature (above 700°C) and low pressure (near atmospheric pressure) [1]. Because low-pressure vessels can be employed instead of a pressurizer and a thick-walled pressure vessel required for high-pressure operation [2], MSRs offer advantages in compactness, resulting in a smaller system volume per unit power. In addition, since the fuel exists in a liquid state, thermal expansion of the fuel salt reduces its density as temperature increases, providing negative reactivity feedback [1].

However, the liquid-fuel characteristic also implies that, in a fuel-salt leakage accident, fission-products (FPs) release can strongly depend on the temperature and flow behavior of the molten salt. In particular, for accident scenarios in which the molten salt is released beyond the primary-system boundary and forms a pool at the bottom of the containment, FPs release characteristics can vary significantly depending on whether a crust exists at the pool boundaries. Therefore, a quantitative assessment of the coolability of a molten-salt pool is essential. Although the total decay heat of a molten-salt pool is lower than that of a typical corium oxide pool, the Rayleigh number can still become sufficiently large due to material-property effects. Consequently, natural convection within the pool can develop strongly and govern heat partitioning to the upper and lower boundaries. Because the local heat flux can vary substantially along the lower boundary [3], the spatial distribution of boundary heat load is an important consideration in containment-vessel design.

Related studies have performed CFD analyses of natural convection, boundary heat flux, and crust behavior in internally heated melt pools using the SST k-ω turbulence model in combination with a solidification/melting model [4]. That work directly simulated crust formation and provided a detailed analysis of heat transfer and phase-change behavior. In contrast, the present study focuses on assessing the feasibility of crust existence under different decay-heat conditions from a containment-design perspective. To this end, rather than directly modeling phase change, we adopt an evaluation procedure that couples boundary heat loads obtained from CFD with a one-dimensional (1D) model.

Accordingly, this study assumes an accident in which the entire inventory of molten salt is released into the MSR containment and forms a pool. The boundary heat load of the resulting molten-salt pool (i.e., the distribution of boundary heat flux) is quantified using CFD and then coupled with a 1D model to efficiently assess crust existence. First, single-phase two-dimensional (2D) axisymmetric CFD simulations are performed under an isothermal boundary condition for three decay-heat levels to obtain the boundary heat-flux distributions. These heat-flux distributions are then applied to a 1D steady-state crust model to evaluate the feasibility of crust existence for each decay-heat condition. For decay-heat conditions in which a crust does not exist, additional CFD simulations are conducted by applying a radiative boundary condition at the pool top and an external cooling boundary condition at the outer surface of the lower containment vessel wall, including wall conduction, and the results are analyzed.

2. Methodology

The objective of this study is to assess whether the interface temperature can be maintained at the melting point under a given decay-heat condition, i.e., to evaluate the feasibility of crust existence. In this work, crust feasibility is defined by whether a positive crust thickness, $\delta_c > 0$, can be obtained from the 1D heat-balance relations (Eq. (1) and Eq. (2)). The overall procedure consists of: (1) computing the boundary heat-flux distribution using CFD, (2) evaluating crust existence using a 1D crust model, and (3) for conditions under which a crust cannot exist, performing additional CFD simulations to assess an external wall-cooling strategy.

2.1. Boundary heat-flux distribution

When a crust exists at a boundary, the melt–crust interface temperature is constrained to the melting point, and the interface can be approximated as an isothermal boundary. Accordingly, to quantify the required heat removal for crust existence, single-phase 2D CFD simulations are conducted by imposing an isothermal condition, $T_s = T_m$, on the pool boundaries. This

approach enables efficient quantification of the heat flux that must be removed to maintain the interface at $T_s = T_m$ without explicitly modeling phase change. It should be noted that the imposed isothermal boundary is not intended to directly represent the actual external heat-transfer environment; rather, it is a modeling setup to determine the required heat flux, q''_{req}, needed to satisfy $T_s = T_m$ at each boundary.

Figure 1 shows the computational domain and boundary conditions. A 2D axisymmetric model is used, and $T_s = T_m$ is applied to each pool boundary. The decay-heat cases are selected as 3 MW, 2 MW, and 1 MW based on the decay-heat curve corresponding to one year of operation. The decay heat is implemented as a spatially uniform volumetric heat source over the entire fluid domain.

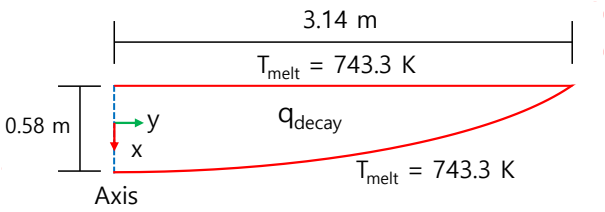

Fig. 1. Computational domain and boundary conditions.

Table I lists the thermophysical properties of NaCl–KCl–UCl_3 used in the CFD simulations. Buoyancy is modeled using a temperature-dependent density. A structured mesh is generated using ANSYS Meshing, and a grid with 34,992 cells is employed. The mesh is designed such that the maximum y^+ remains below 1.

Table II summarizes the numerical settings. The SST k-ω turbulence model is adopted to compute the boundary heat-flux distribution driven by turbulent natural convection. For each decay-heat condition, the boundary heat flux is computed and used as input to the 1D crust model described in Section 2.2.

Table I: Physical properties of NaCl-KCl-UCl_3 for CFD

Properties	**Values**
ρ [kg/m^3]	3476 ~ 2875
C_p [J/kg·K]	609.5 ~ 547.5
k [W/m·K]	0.407 ~ 0.319
μ [kg/m·s]	0.005015 ~ 0.001257
T_{melt} [K]	743.3

Table II: Numerical settings for the isothermal-condition simulations.

Parameters		**Values**
Turbulence model		SST k-ω
Spatial discretization scheme		Body Force Weighted
		2nd order upwind
		1st order upwind
Isothermal condition	Top	743.3 K
	Bottom	
Decay heat		3 MW
		2 MW
		1 MW

2.2. Crust thickness calculation

The boundary heat-flux distribution obtained from the isothermal CFD simulations represents the heat removal required at the boundary to satisfy the imposed condition $T_s = T_m$. In this section, a 1D steady-state crust model is formulated to (i) define the criterion for crust feasibility and (ii) estimate the crust thickness δ_c when crust existence is feasible.

Specifically, the required heat flux obtained in Section 2.1 is mapped to q''_{bot} in Eq. (1) and to q''_{top} in Eq. (2). For given external heat-removal parameters (radiation/convection and, where applicable, an external cooling strategy), the temperatures $(T_1, T_2, T_{\mathrm{top}})$ and the corresponding crust thicknesses $(\delta_{c,\mathrm{bot}}, \delta_{c,\mathrm{top}})$ are determined inversely such that the imposed q'' is satisfied. A positive thickness ($\delta_c > 0$) indicates that crust existence is feasible, whereas $\delta_c \leq 0$, or cases requiring non-physical T_2 or T_{top}, are interpreted as conditions under which a crust cannot exist.

Figure 2 illustrates the heat-transfer pathway at the lower boundary. The lower boundary heat load is transferred through conduction across the crust and the containment wall and is then removed by external convection and radiation. The corresponding steady-state energy balance is given by Eq. (1), where k_c and k_w are the thermal conductivities of the crust and the containment wall, respectively, and $\delta_{c,\mathrm{bot}}$ and δ_w are their thicknesses.

Figure 3 depicts heat transfer at the upper boundary. Here, "solid" denotes a containment internal structure located above the molten-salt pool. Heat from the pool upper boundary is transferred to the structure mainly by radiation, and the energy balance is expressed as Eq. (2).

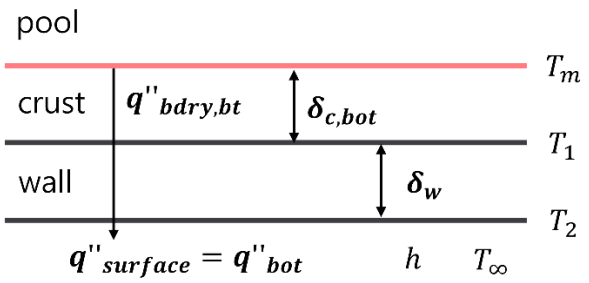

Fig. 2. Schematic of heat transfer at the bottom.

$$q''_{bot} = k_c \frac{T_m - T_1}{\delta_{c,bot}} = k_w \frac{T_1 - T_2}{\delta_w} = h(T_2 - T_\infty) + \varepsilon\sigma\left(T_2^4 - T_\infty^4\right) \quad (1)$$

$$q''_{top} = k_c \frac{T_m - T_{top}}{\delta_{c,top}} = \varepsilon\sigma\left(T_{top}^4 - T_{solid}^4\right) \quad (2)$$

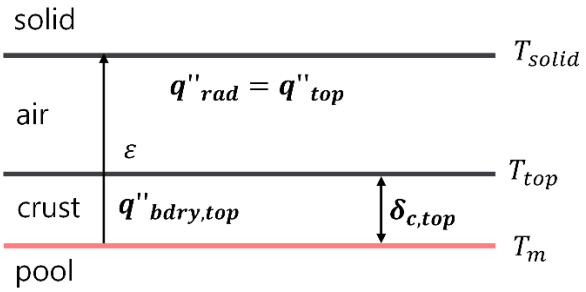

Fig. 3. Schematic of heat transfer at the top.

Table III summarizes the key parameters assumed in the 1D model. The crust thermal conductivity k_c is based on NaCl–KCl–UCl_3 properties, and k_w corresponds to SS316. For the lower boundary, the external heat-transfer coefficient is set to 25 W/m^2·K, representing natural convection of air, and the ambient temperature is assumed to be 55 °C. For the upper boundary, the emissivity is set to 0.5 and the structure temperature is also assumed to be 55 °C.

Table III: Assume values for 1D model

Paramters	Values
T_∞ [K, ℃]	328.15, 55
k_c [W/m·K]	0.4
k_w [W/m·K]	20
h [W/m^2·K]	25
δ_w [m]	0.1
σ [W/m^2·K^4]	5.67×10^{-8}
T_{solid} [K, ℃]	328.15, 55
ε (emissivity)	0.5

2.3. Crust thickness calculation

Sections 2.1–2.2 quantify the required heat flux to maintain $T_s = T_m$ and assess crust feasibility using the 1D model. In Section 2.3, additional CFD simulations are performed under more realistic external heat-transfer conditions to evaluate whether external wall cooling can reduce the upper-boundary heat load and q''_{top} sufficiently to enable crust existence. In these simulations, a radiative boundary condition is applied at the pool top, while a water-cooling boundary condition is imposed on the outer surface of the lower containment wall. To account for wall conduction, the computational model includes a 100 mm-thick containment wall made of SS316 (properties summarized in Table IV). Table V lists the numerical settings used for the external cooling cases. The water cooling is represented using an equivalent heat-transfer coefficient of 1000 W/m^2·K, and the bulk temperature is set to 373.15 K (100 °C), reflecting the boiling point of water.

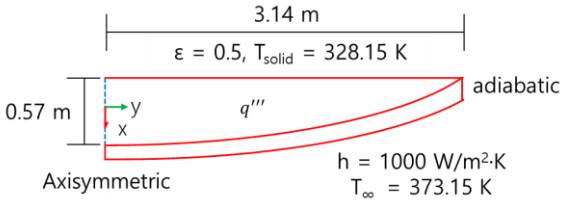

Fig. 4. Computational domain and boundary conditions for external cooling conditions

Table IVV: Properties of SS316[5]

Properties	Values
ρ [kg/m^3]	7900
C_p [J/kg·K]	459.292+0.132891×T
k [W/m·K]	9.248+0.01571×T

Table V: Numerical analysis for external cooling conditions

Parameters		Values
Turbulence model		SST k-ω
Spatial discretization scheme		Body Force Weighted
		2nd order upwind
		1st order upwind
External cooling condition	Top	ε = 0.5 Tsolid = 328.15 K
	Bottom wall	h = 1000 W/m2·K T_∞ = 373.15 K
Decay heat		3 MW
		2 MW

3. Results

Figure 5 compares the angular distributions of the boundary heat flux at the upper and lower pool boundaries for each decay-heat condition. At the upper boundary, the heat flux decreases with increasing distance from the pool center for all three decay-heat levels. In contrast, at the lower boundary, the heat flux shows an increasing trend as the angle increases away from the pool center.

3.2. Crust thickness

Based on Eq. (1), the lower-boundary crust thickness was evaluated for the three decay-heat conditions. For all cases, a crust was predicted only within the region where the angle is below 10°; no crust was obtained for angles greater than 10°. The upper-boundary crust thickness was evaluated using Eq. (2), and the results indicate that no crust exists at the upper boundary for any of the three decay-heat conditions.

3.3. Required cooling conditions

External wall-cooling simulations were performed for representative conditions (3 MW and 2 MW) among those identified by the 1D model as having no upper-boundary crust. Figure X presents the temperature field of the molten-salt pool under the external cooling

boundary condition. Although the lower region of the pool and the near-wall region become cooler due to external wall cooling, the upper pool region remains at a relatively high temperature. The upper-boundary temperature does not drop below the melting temperature assumed in this study (T_{melt}); therefore, the present external wall-cooling condition alone is not sufficient to sustain an upper-boundary crust.

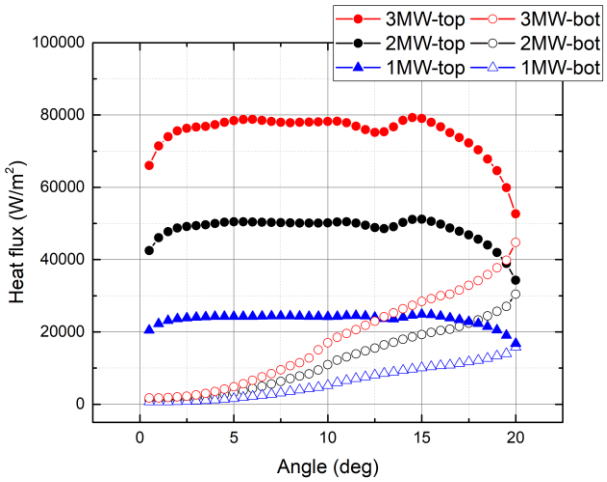

Fig. **5**. Comparison of heat flux at top and bottom boundaries by decay heat.

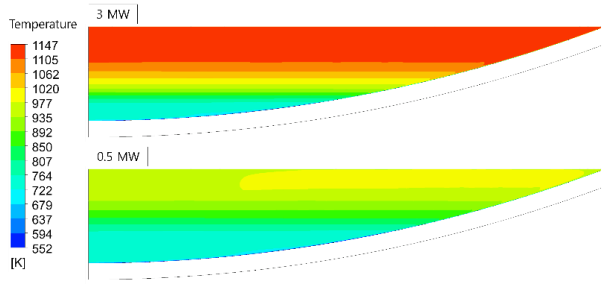

Fig. **6**. Temperature field of the molten-salt pool under the external cooling boundary condition.

4. Conclusion

This study considers an accident scenario in which molten salt is released into MSR containment and forms a pool. The boundary heat load of the pool was quantified using 2D CFD for different decay-heat conditions, and crust feasibility was evaluated by coupling the CFD results with a 1D crust model. In addition, for conditions under which crust existence is difficult, additional CFD simulations with external wall cooling were conducted to examine the feasibility of sustaining an upper-boundary crust. The main conclusions are summarized as follows:

1) Using CFD with an isothermal boundary condition ($T_s = T_{melt}$), the required boundary heat-flux distributions were obtained for each decay-heat condition. The lower-boundary heat flux exhibited a clear spatial dependence with respect to the angular position, highlighting the importance of evaluating local boundary heat loads from a containment-design perspective.

2) From the Eq. (1)-based assessment of the lower-boundary crust thickness, a crust was feasible only in a limited region ($\theta \leq 10°$) for all three decay-heat conditions (3 MW, 2 MW, and 1 MW), whereas no crust was obtained for $\theta > 10°$. This indicates that a globally sustained lower-boundary crust is difficult to achieve and that crust existence may be limited to localized regions.

3) From the Eq. (2)-based assessment of the upper-boundary crust thickness, no upper-boundary crust was obtained for any of the three decay-heat conditions. Under the assumptions adopted in this study, radiative heat removal at the top alone is not sufficient to sustain a crust, suggesting that additional heat-removal strategies are required to enable an upper-boundary crust.

4) For the 3 MW and 2 MW cases with external wall cooling, the temperature in the lower and near-wall regions decreased; however, the upper-boundary temperature still did not fall below T_{melt} for either case. Therefore, lower external wall cooling alone may be insufficient to secure an upper-boundary crust, and further measures to enhance heat removal at the top are needed.

Future work will quantify the sensitivity of the boundary heat load to turbulence-model selection and will expand the range of containment geometry and external cooling conditions to develop design options for sustaining an upper-boundary crust.

ACKNOWLEDGMENTS

This research was supported by the National Research Foundation of Korea (NRF) and funded by the ministry of Science, ICT, and Future Planning, Republic of Korea (grant numbers RS-2021-NR056168), and the Human Resources Development of the Korea Institute of Energy Technology Evaluation and Planning (KETEP) grant funded by the Korea government Ministry of Knowledge Economy (RS-2024-00439210).

REFERENCES

[1] J. Serp, M. Allibert, O. Beneš, S. Delpech, O. Feynberg, V. Ghetta, D. Heuer, D. Holcomb, V. Ignatiev, J. L. Kloosterman, L. Luzzi, E. Merle-Lucotte, J. Uhlíř, R. Yoshioka, and D. Zhimin, The Molten Salt Reactor (MSR) in Generation IV: Overview and Perspectives, Progress in Nuclear Energy, Vol. 77, pp. 308-319, 2014.

[2] D. LeBlanc, Molten Salt Reactors: A New Beginning for an Old Idea, Nuclear Engineering and Design, Vol. 240, No. 6, pp. 1644-1656, 2010.

[3] T. G. Theofanous, C. Liu, S. Additon, S. Angelini, O. Kymäläinen, and T. Salmassi, In-vessel coolability

and retention of a core melt, Nuclear Engineering and Design, Vol. 169, Issues 1–3, pp. 1–48, 1997.

[4] A. Venkateshwaran, M. Kumar, S. Kumar, A. Joshi, and C. Pain, Numerical study of the effect of geometry on the behaviour of internally heated melt pools for in-vessel melt retention, Progress in Nuclear Energy, Vol. 156, 104555, 2023.

[5] C. S. Kim, Thermophysical Properties of Stainless Steels, Argonne National Lab., Ill. (USA), No. ANL-75-55, 1975.